DEVELOPMENT OF NICKEL DOPED NANO HYDROXYAPATITE AS PROANGIOGENIC MATERIAL FOR BONE TISSUE ENGINEERING

A PROJECT SUBMITTED IN PARTIAL FULFILLMENT OF THE REQUIREMENTS

FOR THE DEGREE OF

Master of Technology

In

Biotechnology

By

ANU PRIYA B

213BM2018

Under the Supervision of

Dr. INDRANIL BANERJEE

Department of Biotechnology and Medical Engineering

National Institute of Technology

Rourkela-769008, Orissa, India

May 2014

CERTIFICATE

This is to certify that the research project report entitled "**Development of nickel doped nano hydroxyapatite as proangiogenic material for bone tissue engineering**" submitted by **Anu Priya B**, in partial fulfilment of the requirements for the award of the Degree of Master of Technology in Biotechnology and Medical Engineering with specialization in Biotechnology at National Institute of Technology Rourkela is an authentic work carried out by her under my supervision and guidance.

To the best of my knowledge, the matter embodied in the thesis has not been submitted to any other University/ Institute for the award of any Degree or Diploma.

Dr. Indranil Banerjee

Assistant Professor

Department of Biotechnology and Medical Engineering

National Institute of Technology, Rourkela

ACKNOWLEDGEMENTS

I take this opportunity to express my gratitude and heartfelt thanks to every individual who has taken part in my Report since from the inception of the idea to completion.

I am privileged to express my deep sense of gratitude and profound regards to my supervisor **Dr. I. Banerjee**, Asst. Professor, Department of Biotechnology and Medical Engineering, N.I.T Rourkela for his esteem guidance and noble supervision during the hours of the project since from the needs of the project to results of it.

I am also thankful to **Head of the department, Prof. Krishna Pramanik** and all the faculty members of the department of biotechnology and medical engineering, for extending their cooperation and helping hand in completing my project work.

Further, I would like to express my thankfulness to **Prof. K. Pal** for their help and providing access to their lab.

I consider it a privilege to express my gratefulness to **Prof.T.K.Maiti**, **Department of Biotechnology, Indian Institute of Technology Kharagpur** and **PSG Institute of Advanced Studies** for providing me with molecular laboratory facility and and HR-TEM facility, respectively.

I also would like thank **Mr. K. Senthil guru, Mr. S.N. Gautham Hari Narayana, Mr. Soham Mukherjee** for their constant encouragement and for their day-to-day support.

Finally, I would like to express my love and respect to my parents **Mr. G. Bharathi Rajan and Mrs. B. Nagalakshmi**, family and friends for their encouragement and endless support that helped me at every step of life. Their sincere blessings and wishes have enabled me to complete my work successfully.

Anu Priya B
213BM2018
M.Tech. Biotechnology
Department of Biotechnology and Medical Engineering

TABLE OF CONTENTS

ABSTRACT

Induction of angiogenesis within the artificial bone graft after implantation is of paramount importance in the field of bone tissue engineering. For this purpose, here, we are developing nickel ion doped nHAp which improves angiogenesis. nHAp doped with varying concentrations of nickel were prepared using wet chemical precipitation method using cationic surfactant (CTAB) as a template and the extent of doping was studied using EDAX. The prepared particles with ferret diameter of 15-17 nm (TEM analysis), showed almost similar surface area for all samples (using BET analysis) but there was an increase in surface charge observed as the doping increases (ZETA potential). Crystalline nature of doped hydroxyapatite particles were studied using XRD and FTIR. Detailed analysis relevant to the bone cells (Mg-63) proliferation and differentiation showed that doping of nickel to hydroxyapatite supports cell growth and proliferation (MTT, live dead assay and cell cycle analysis) and also differentiation of these cells which were analysed using *in vitro* Runx2 expression and bone nodule formation by SEM study. VEGF expression by ELISA and HIF-1α expression studies revealed that doping of nickel greatly supports angiogenesis. This confirms that nickel ion doped hydroxyapatite improves angiogenesis along with osteogenesis pinpointing its potential in bone tissue engineering application.

List of Tables

List of figures

CHAPTER 1

INTRODUCTION AND LITERATURE REVIEW

1.1. Biology of bone:

1.1.2. Bone structure:

There are generally two types of bone found in human body: trabecular and cortical bone. Cortical bones make up to 80 % of the total skeleton and are hard and compact but not much porous (flat bones and outer part of long bones). These bones have mineralised compartment and provides mechanical strength. On the other hand, trabecular bones (cancelous or spongy bones) make up to 20 % of the total skeleton and are highly porous arranged in a honeycomb-like rods of various sizes called trabeculae. These cancelous bones are fully vascularized and help in the metabolic functions[1].

1.1.3. Bone cells:

a) Osteoblasts – These are bone forming cells which initially form non-mineralized osteoids and later differentiate into osteocytes (mature osteoblasts) that gets embedded in the bone matrix. Osteoblasts are generally found in the cancelous bones where the metabolic rate is higher[2].

b) Osteoclasts – These multinucleated cells helps in bone resorption by degrading the organic component and dissolving the mineral component of the bone matrix when needed[2].

c) Osteocytes – These are the terminally differentiated cells which play a role in the normal metabolism of bone by transducing signals from mechanical stress, secreting necessary enzymes, controlling bone mineral content and release of calcium ions into the blood[2].

1.1.4. Bone formation and remodelling:

The formation of new bone is initiated with the process called cellular condensation in which the mesenchymal cells migrate from different parts and proliferate. Differentiation of the mesenchymal stem cells into pre-osteoblasts and osteoblasts occurs via one of the two mechanisms: endochondral ossification and intramembranous ossification. In endochondral ossification, the cartilage plate is first formed which gets replaced by the bone later, and mostly bone formation is through this process. In intramembranous ossification, mesenchymal stem cells directly differentiate into pre-osteoblasts and osteoblasts, and this mechanism occurs primarily in flat bones of the skull, scapula and mandible[3].

Bone is a connective tissue which undergoes continuous remodelling to maintain structural integrity. Remodelling of bone consists of two steps: bone resorption followed by new bone formation. During bone resorption, osteoclasts attach to the old and damaged bone surface and initiates the degradation of bone matrix by releasing factors. Osteoblasts then fill up the resorption area and helps in bone mineralization and formation of the new bone matrix. In a healthy bone, this process of resorption and formation in remodelling is very well co-ordinated and balanced[4].

1.2. Need for bone tissue engineering:

Many bone related diseases like osteoporosis and osteoarthritis, genetic disorders like osteogenesis imperfecta and bone fractures need treatments which help in regeneration of bones. As the rate of bone defects and diseases increases, the need for bone substitutes also increases in the field of the orthopaedic health sector. One of the major concern is the proper integration of the bone substitutes with its natural counterpart. Conventional methods of treatment include the use of autografts and allografts that can integrate with the existing bones perfectly. But they come with limitations such as scarcity of donors, immunorejection,

donor site morbidity, severe pain and risk of infections and high chances of transmission of diseases (in case of allografts)[5]. These limitations gave way for the artificial prostheses for bone fractures (one of the major application of artificial prostheses is the use in hip bone fracture) but then the wearing of the implant material at times leads to the death of the bone cells at the site of fracture and also there won't be any bonding between the chemically inert prostheses and the biological tissue. These limitations opened the door for the field of bone tissue engineering which uses a wide range of polymeric and ceramic scaffolds that fits perfectly into the bone defects and helps in osteointegration[6].

1.3. Bone tissue engineering – current trends:

The focus of bone tissue engineering field is on creating bone constructs that are capable of improving the osteogenesis in the site of the bone defect. Bone constructs are implanted by seeding the cells with osteogenic potential into the biodegradable scaffolds in vitro and directly transplanting *in vivo* to assess their potential in the formation of bone. Another kind of bone construct is that after cell seeding into the scaffolds, they were cultured *in vitro* to form mature bone-like grafts which are then implanted. The structural properties of the scaffold have a great influence on the cell growth and proliferation. Bone tissue scaffolds after implantation should have a macrostructure mimicking the physiological function of the matrix to maintain the cell's natural phenotype. Porosity and interconnectivity of the scaffold (70-80 %) is also necessary for promoting tissue ingrowth and vascularization from surrounding tissues and also for the removal of the metabolic waste that has penetrated the scaffold from the surrounding cells. Most importantly scaffold should be bio-compatible and bio-degradable[7].

1.4. Biomaterials for bone tissue engineering:

For a successful implantation, the scaffold should be highly biocompatible. The selected scaffold material should also degrade and resorb at a controllable rate at the same time as the specific tissue cells seeded into the construct attach, spread and increase in quantity as well as quality[8]. The design and fabrication of scaffolds in tissue engineering are driven by two main categories: polymers and ceramics.

1.4.1. Polymeric biomaterials:

Because of ease of design modification and surface modification, a variety of polymers have been used to fabricate scaffold. Generally two categories of polymers are found: biodegradable and non-biodegradable polymers. Biodegradable polymers are generally used for making scaffolds, and they have good mechanical properties and degrade at a controllable rate. Poly lactic acid (PLA), poly glycolic acid (PGA), collagen and co-poly L-lactide (CPLA) are some of the examples of biodegradable polymers. One of the important limitations of biodegradable polymers is that endothelial cells cannot adhere to these materials[9]. This gave opportunity for ceramic biomaterial for the application as scaffolds for bone tissue engineering.

1.4.2. Ceramic biomaterials:

Ceramic biomaterials based scaffolds are composed of metallic and non-metallic elements and inorganic ceramic materials. They have good mechanical behaviour such as hardness. However they are very brittle, requiring less energy to fracture. They can be bioinert, bioactive or bioresorbable. They do not bond with the bone, instead tissue ingrowth into ceramic pores happens. Bioactive ceramics is generally used for bone tissue engineering application and evoke biological response at bone tissue implant surface by exchange of ions to form a bond between the host tissue and the biomaterial. They can also be used as coating

on other non-bioactive materials such as metals to induce a strong biological fixation between the host tissue and implant material[10].

1.4.3. Hydroxyapatite:

Hydroxyapatite, with the chemical formulae $Ca_{10}(PO_4)_6(OH)_2$ is one such bioactive ceramic which is chemically similar to the inorganic phase of natural bone and used widely in bone tissue engineering. It is chemically stable at acidity levels less than 4.3 (which is the pH of blood)[11]. Much like calcium phosphates, HAp also has osteoconductive and osteoinductive properties. Bioactivity is related to a modification of the surface of the HAp material. Its bioactivity has been seen to be affected by structural crystallinity. The theortical mole ratio of Ca and P in HAp is 1.67. However, this is not the value observed in the organism because small amounts of carbon, nitrogen, iron and other elements are also incorporated. In the hexagonal systems, the hydroxyl ions (OH^-) are located at the centre of Ca^{+2} triangles along the c-axes of the hexagonal unit cell. The OH- ions are aligned in columns parallel to the c-axis along with Ca^{+2} and (PO_4^{-3}) ions. There are various parameters to be considered for usage of hydroxyapatite such as size, morphology, appropriate stoichiometry, phase composition and crystallinity. HAp is composed of strongly bonded, large crystal structures with smaller surface areas than the nano-sixzed, weakly bonded bone mineral crystals therefore reducing the rate of particle disintegration and crystal dissolution of the implant[12]. In particular, the high stability and flexibility of the apatite structure accounts for the great variety of possible cationic and anionic substitutions. Therefore, metal and ion substituted hydroxyapatite is very much used in bone tissue engineering applications nowadays.

1.5. Vascularization of bone grafts:

For the engineered bone tissue to survive and integrate properly, vascularization is a requisite after implantation as it is necessary for the efficient oxygen and nutrition exchange between

the tissue. One of the drawbacks in implantation is that the molecular diffusion of oxygen and nutrients is limited over a short range of 150 – 200 μm and diffusional transport more than that distance results in acellular regions. Even though cell survival can be enhanced by using larger scaffolds, vascularization of the implant need to be considered for the successful implantation of the bone construct[13].

1.6. Present strategies for improving vascularization in bone tissue constructs:

Vascularization in bone tissue engineering is of utmost importance for the proper supply of oxygen, nutrients and growth factors thereby enhancing the new bone formation. To date, many strategies have been administered for the improvement of vascularization in bone tissue constructs. They are: i) growth factor delivery ii) co-culturing systems iii) gene delivery iv) development of microfluidic based network inside the scaffold v) using biomaterials with appropriate properties.

1.6.1. Growth factor delivery:

Cells communicate with each other via a cascade of signalling molecules (growth factors and proteins) to mediate cellular functions and also migration, proliferation and differentiation of cells. Some of the growth factors involved in the bone formation are: VEGF (vascular endothelial growth factor), FGF (fibroblast growth factor), PDGF (platelet derived growth factor), IGF (insulin-like growth factor), ET-1 (endothelin-1), ET-2 (endothelin-2), BMP-2 (bone morphogenetic protein-2), BMP-7 (bone morphogenetic protein-7), TGF-β (transforming growth factor-β). In the bone micro environment, there is always a cross talk between the bone cells and the endothelial cells present in the surrounding blood vessels. For instance, VEGF produced by osteoblasts help in promoting angiogenesis in endothelial cells and BMP's released by the endothelial cells help in osteogenic differentiation. Numerous researchers around the world working in the field of bone tissue engineering have tried to

incorporate the idea of delivering exogenous growth factors to control the cellular behaviour both *in vitro* and *in vivo*. But there are many disadvantages. Firstly, delivery of single growth factor alone cannot elicit a complete regeneration of bone. Secondly, this approach leads to the nonlocalized delivery of growth factors and transient cellular responses. Finally growth factor delivery is time and dose dependent[14].

1.6.2. Culturing Endothelial cells inside the scaffold:

Another novel approach is to introduce endothelial cells or its progenitors directly into the scaffold. But this method has its drawback as there is only one cell type used and it is difficult to develop a complete vascularized tissue as the growth factors and signals from other cell types (in this case, bone cells) won't be present. Also, it is an essential from which source the endothelial cells are taken as its angiogenic nature depends on the source[15]

1.6.3. Co-culturing system:

By now it is understood that both angiogenesis and osteogenesis plays a role in the bone formation *in vivo.* Angiogenesis is one of the requisites for the osteogenic differentiation as it helps in the migration of osteoblast precursor cells to the site of bone formation. *Zhou et al.,* and *Villers et al.,* in their research found that co-culturing of human mesenchymal stem cells (MSCs) and endothelial cells (ECs) within the biomaterial β-TCP resulted in the formation of vascularized bone tissue. Similarly, *Wang et al.,* demonstrated that the co-culturing of human osteoblast-like cells and human umblical vein endothelial cells resulted in new bone formation with blood vessels. However, the co-culturing system becomes more complex to study and understand. Also research on co-culture system to date are very conflicting as in few studies though they showed the vessel formation there was no evidence for the integrity and functionality of the vessels within the grafts (*Fuchs et al.,* and *Rouwkema et al.,*)[15].

1.6.4. Gene delivery:

Limitations of gene delivery include: i) safety concerns for viral gene deliveries ii) non-viral delivery faces the problem of insufficient transport of pDNA into the nucleus and iii) lastly, many clinical trials of gene deliveries failed[16].

1.6.5. Development of microfluidic based network:

Recent advancement in this field is the development of microfluidic based network for vascularization within the scaffold. These microfluidic channels mimic the micro vasculatures present surrounding the bone. Growing the endothelial cells within these microfluidic networks helped in developing the 3D vascular network within the scaffold. Even though this system is gaining much attention, it is very difficult to create such a complex array of system as it requires much sophisticated system and costly infrastructure and also it is very important to study the nature of the materials used for creating such channels[17].

1.7. Development of pro-angiogenic biomaterial:

Nowadays, development of pro-angiogneic biomaterial is gaining much attention as it triggers the cells to produce vast quantities of angiogenic factors *in vivo* which is normally achieved by creating tissue hypoxic condition *in vivo*. It is already a known fact that hypoxia (decreased oxygen level) is one of the potent inducers of angiogenesis. Here, hypoxia inducible factor – 1α (HIF-1α) is the key regulator of angiogenesis. HIF-1 consists of two subunits: HIF-1β and HIF-1α. HIF-1β (also called aryl hydrocarbon receptor nuclear translocator (ARNT)) is constantly expressed and present within the nucleus. On the other hand, HIF-1α is present in the cytosolic region, and it is oxygen sensitive. Under the normoxic condition, HIF-1α undergoes prolyl hydroxylation by the enzyme prolyl

hydroxylase (PHD) (which becomes active when its co-factors iron, 2-oxoglutarate and oxygen gets bound to it). Von-Hippel-Lindau protein (E3 ubiquitin ligase) then initiates its proteosomal degradation. But under hypoxic condition, since prolyl hydroxylase cannot be activated, accumulation of HIF-1α happens which moves into the nucleus and forms dimer with HIF-1β subunit which forms a complex with co-activator p-300 and trans activates the HIF-1 responsive genes by binding to the hypoxia responsive elements (HRE) region in those genes. One such gene is VEGF, which in turn activates the VEGF protein (a potent mitogen) that helps in the migration and proliferation of endothelial cells forming tubular structures. Also, it is known that in the bone remodelling compartment, expression of VEGF helps in osteoblast and osteoclast differentiation thereby enhancing the bone resorption and bone formation[18]. It is quite evident from the previous researches that even under normoxia, metal ions like nickel, cobalt, and copper inactivates the PHD enzyme by replacing iron (a co-factor required for the activation of PHD) which thereby stabilizes HIF-1α. *Wu et al.*, exploited these strategies and showed that copper and cobalt doped mesoporous bioactive glass scaffolds can effectively induce cellular VEGF production and angiogenesis[19, 20]. But the stabilization of HIF-1α and subsequent activation of VEGF was very strong in the case of nickel ions. Therefore, we hypothesize to incorporate nickel in a biomaterial to exploit this area. However, high concentration of nickel may induce nickel toxicity. So a controlled ion release system is very much essential for vascularized bone tissue engineering strategy.

CHAPTER 2

OBJECTIVES AND WORK PLAN

2.1. Objectives:

To prepare and physicochemically characterize nickel doped nano hydroxyapatite. Further biologically characterize the prepared nickel doped nano hydroxyapatite to evaluate the osteogenic and angiogenic property of the material invitro.

2.2. Work Plan:

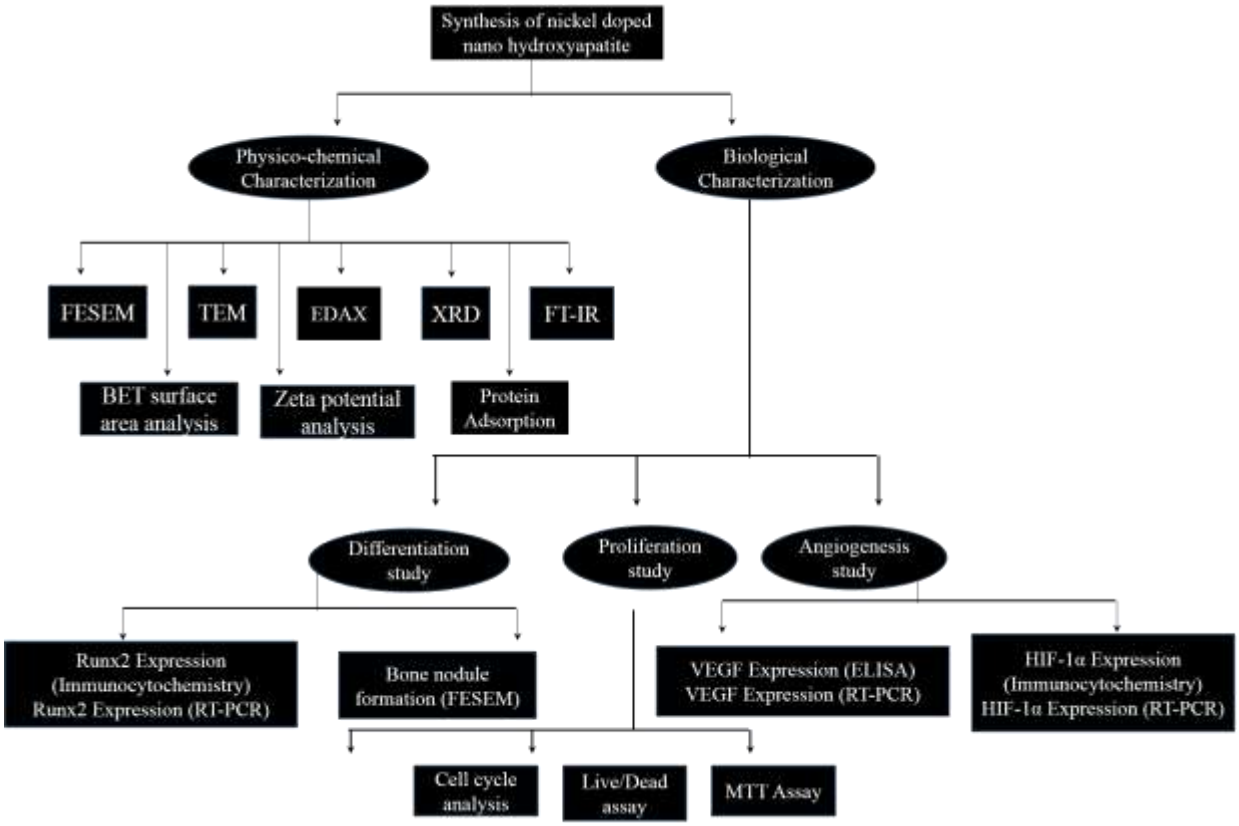

2.3. Rationale:

As the scope of bone tissue engineering is rising in most parts of the world, the need for vascularization of the bone grafts is of paramount importance for successful implantation. Although there are many pre-vascularization techniques available, they come with their limitations. Hence this study is aimed at developing a pre-angiogenic nickel doped nano hydroxyapatite for bone tissue engineering application.

CHAPTER 3

MATERIALS AND METHODS

3.1. Materials:

Calcium nitrate tetrahydrate ($Ca(NO_3)_2.4H_2O$), diammonium hydrogen phosphate ($(NH_4)_2HPO_4$), nickel nitrate hexahydrate ($Ni(NO_3)_2.6H_2O$), cetyltrimethylammonium bromide (CTAB) and ammonia solution (25%) were purchased from Merck, India. Dulbecco's Modified Essential Media (DMEM), Dulbecco's Phosphate Buffer Saline (DPBS) solution, Trypsin-EDTA solution, Fetal Bovine Serum, antibiotic-antimycotic solution, and MTT assay kit were purchased from Himedia, India. Human VEGF ELISA kit was purchased from Abcam, UK. mRNA isolation kit (RNeasy Mini) and cDNA synthesis kit (MuLV Reverse Transcriptase Plus Kit) were bought from Qiagen and BioBharti LifeSciences Pvt. Ltd., India, respectively. The MG-63 cell line was procured from NCCS, India.

3.2. Synthesis of nano-hydroxyapatite and nickel doped nano-hydroxyapatite:

The well-known wet chemical precipitation method was employed here to synthesis the hydroxyapatite[21]. In this method, 200 ml of 0.05M Calcium nitrate tetrahydrate was taken in a beaker and placed in a sonicator bath at 80°C and the pH of the system was maintained at 10-12 by addition of ammonium hydroxide. To this solution, 200ml of solution containing 0.03M diammonium hydrogen phosphate and cetyltrimethylammonium bromide (CTAB) in the ratio 1:1 was added drop-wise at a constant flow rate of approximately 1.5ml/min from a burette. The slurry was allowed to age for 24 hours and then repeated washing was done by centrifuging at 6000 RPM for 10 minutes to remove the ammonia byproducts and unwanted CTAB. The precipitate was then dried at 55°C for 24 hours to get the HAP powders. Nickel doped nano-hydroxyapatite samples were prepared using the above method in which different doping percentage of Nickel(II) nitrate hexahydrate(1%, 5%, and 10%) was first added to the calcium nitrate solution and then reaction was started. The molar ratio of Ca/P in all the cases were maintained at 1.67.

3.3. XRD and FT-IR:

The phase content of the samples was studied using XRD method. Philips XRD-PW1700, Rockville USA instrument was used for this analysis. The scanning was done over a range of $2\theta = 20°\text{-}60°$ at a scanning rate of 2° per minute[22].

FTIR analysis was done to determine the functional groups present in the HAP Samples. It was performed using an AKTR FTIR Spectrophotometer instrument with the scanning range of 400 cm^{-1}-4000cm^{-1}, and the pellets were obtained using the KBr pelleting technique[23].

3.4. TEM and EDAX:

JOEL JEM 2100 High –Resolution Transmission Electron Microscope (HR-TEM) was used to determine the nature of the synthesized HAP particles. Sample specimen were prepare using Copper grid with Formware –C Coating[24].

EDAX analysis was performed to determine the amount of nickel doped onto each sample[25].

3.5. BET and Zeta Potential Analysis:

BET surface area analyser (Quantachrome Instruments) was used to determine the surface area, pore size and pore volume of the synthesized HAP particles the analysis was done at 5-point fast scan[26].

The ZETA potential of the HAP samples was determined using Marvelin DLS and ZETA analyser using water as the dispersion medium. The samples were dispersed in10 ml of water taken in a test tube and sonicated for 10 -15 min so that there wont be any agglomeration of HAP particles[27].

3.6. Protein Adsorption Study:

The adsorption of proteins by the samples can be studied by comparing it with the adsorption of BSA (Bovine Serum Albumin) by the samples. The residual protein concentration in the supernatant was determined using Bradford assay. The adsorption of the proteins by the samples were determined by subtracting the residual protein concentration from total protein concentration[28].

3.7. Cytocompatibility Study:

Cell proliferation of the samples were studied using MTT Assay on MG-63 cell line (from NCCS, Pune, India). 1 x 10^4 cells/well were added in 96 well plate and incubated for 24 hrs for the cells to adhere properly. After 24 hours of incubation, the cells were treated with HAP samples at a concentration of 100µg/ml and then again incubated. After 1^{st}, 3^{rd} and 5^{th}day, MTT assay was performed[29].

Cell cycle analysis was performed used FACS. 1 X 10^6 cells were seeded into 6 well plate and then treated with the samples at a concentration of 100µg/ml and then incubated. After 24 hours of sample treatment, the cells were trypsinized, washed with ice cold PBS and then fixed with 70% ice cold ethanol. After 24 hours, fixed cells were centrifuged at 3000RPM and the pellets were suspended in 100µl of PBS and 500µl of PI staining dye and then allowed to stain for 30 min at room temperature[]. The samples were then analyzed using FACS Accuri C6 (BD Biosciences)[30].

Live/Dead assay was perfoemed using FACS for cell viability study. 5 X 10^5 MG-63 cells were seeded onto the 6 well plate and left for adhereing at 37°C, 5% CO_2 and 95% humidity. After 12 hours of incubation, the cells were treated with 100µg/ml of sample and further incubated. After one day of sample addition, the cells were trypsinized (also the supernatant was taken) and washed with ice cold PBS and then suspended in 500µl of PI

buffer (50µg/ml PI and 100 U/ml RNase) and incubated for 30 min at room temperature[31]. The samples were analysed using FACS Accuri C6 (BD Biosciences). The same protocol was followed to determine the amount of live cells on day 3 and day 5.

3.8. FESEM study

Field Emission Scanning Electron Microscopy (TOEL India TSM 6480 LV) was used to determine the effect of the samples on MG-63 cells. 5 X 10^4 cells were seeded onto the glass slides kept inside each well of the 12 well plate and left to adhere for 12 hours in the incubator at 37°C, 5% CO_2. Thereafter, the cells were treated with the samples at a concentration of 100µg/ml and incubated at 37°C, 5% CO_2. After 3 days of sample treatment, the cells were taken out and washed with SEM buffer at pH 7.2 (3 X 5min) and fixed with SEM grade gluteraldehyde for 2 hours. After 2 hours, the cells were again washed and fixed with osmium tetroxide for 2 hours. The cells were then washed and serially dehydrated with ethanol from 30% -100 % each (10 min) and then allowed to dry[32].

3.9. Expression of Runx2 and HIF-1α

Expression of the differentiation marker Runx2 and angiogenic promoter HIF-1α was studied using immunocytochemistry analysis.5 X 10^4 MG-63 cells were seeded and incubated at 37°C, 5% CO_2 and 95% humidity for the cells to adhere properly. After the incubation period, the standard ICC protocol was followed. The cells were fixed with 4% paraformaldehyde (10 min, room temperature), permeabilized with permeabilization buffer (PBS with 0.25% TritonX) for 10 min at room temperature and then incubated with blocking buffer (1% BSA in PBST + 0.3M Glycine) for 30 min at room temperature to block any unspecific binding of the antibodies. After this, the cells were incubated for 1 hour at room temperature with the primary antibody which was followed by washing with PBS (3 X 5min) then incubated with secondary antibody tagged with Alexa Flour 488 (1:1000 dilution) for 1

hour at room temperature. Further, the cells were washed again with PBS (3 X 5min), stained with TRITC (tetramethylrhodamineisothiocyanate) phalloidin and Hoechst dyes to view under confocal microscope (TCS-SP8, Leica, Germany)[33].

3.10. VEGF Expression Study:

Expression of VEGF was determined using human VEGF ELISA kit (Abcam 100662). For this purpose, 2 X 10^5 MG-63 cells were seeded onto a 12 well plate and incubated at 37°C, 5% CO_2 and 95% humidity for the cells to adhere properly. After 12 hours of incubation, the cells were treated with 100µg/ml of samples. After 48 hours of sample treatment, the supernatant was transferred to a sterile vial and then ELISA was performed as mentioned in the protocol from the kit. To summarize the process, 100µl of the samples were added to the 8-well ELISA plate which were pre-coated with VEGF capture antibody and incubated for 2.5 hours which was followed by washing, incubation with 100µl of 1X biotinylated VEGF detection antibody for 1 hour, subsequent washing and then incubation with 100µl of 1X HRP Streptavidin solution for 45min at room temperature. Further, it was incubated with 100µl of TMB onestep substrate reagent for 30 min at room temperature for the colour development. Subsequently stop solution was added, and the absorbance was measured at 450nm[33].

3.16. RT-PCR analysis:

Expression of VEGF, Runx2, HIF-1α was checked using RT-PCR. For this purpose 1 x 10^6 cells were seeded on to each well of a 6-well plate and cultured following the protocol mentioned above. After 24 h of incubation, samples (100µg/ml) were added to the cells, and it was further incubated for 48 h. After incubations, cells were lysed using lysis buffer. Extraction of mRNA from the cell lysate was done using RNA isolation kit (QIAGEN RNeasy Mini Kit) following the manual provided by the supplier. At the end of the process,

the concentration of mRNA was estimated spectrophotometrically (Nanodrop) and appropriate dilution was made to keep the mRNA concentration same for all the samples. Then mRNA were converted to cDNA and subjected to PCR using BioBharti MuLV ReverseTranscriptase Plus Kit. For PCR, cDNA were mixed with primers (listed below) and 'PCR mix' following appropriate stoichiometry as per the instruction given in the manual. After completion of the PCR, sample were analyzed using 1.5 % agarose gel[34].

CHAPTER 4

RESULTS AND DISCUSSION

4.1. Preparation of Ni^{+2} doped nano hydroxyapatite

Synthesis of nano hydroxy apatite and Ni^{+2} doped nano hydroxy apatite was done by ammoniacal precipitation method (Table.1 and Fig.1). To control the size of the nanoparticle, a cationic surfactant CTAB was used as a capping agent [35]. Three different Ni^{+2} doped nano hydroxy apatite samples were prepared by varying the doping concentration. The yield of nano HAp powder was between ~ 0.9 to 1.0 g in all the cases. To break the agglomerate of the synthesized nano hydroxy apatite, the dried samples were ball- milled. Physical inspection of the powder revealed that all powders were free flowing. Pure nano hydroxy apatite was white coloured, but the colour changed from white to whitish- green with Ni doping because of hexaaquanickel ion[36].) and Yan Li *et al.,* (2010) when they doped Co^{+2} and Cu^{+2}, respectively in hydroxyapatite [25, 37].

Table 1. Composition, yield and physical appearance of nHAp and Ni^{+2} doped nHAp

S.No	Samples	Composition	$[Ca(NO_3)_2.4H_2O + Ni(NO_3)_2.6H_2O]$	$(NH_4)_2HPO_4$ g/200ml	Yield (g)	Colour
1.	HAI					Milk White
2.	N1-HA					reamy White
3.	N5-HA					eenish White
4.	N10-H	10%(w/w)Nickel [(Ca+Ni)/P: 1.67]				eenish White

Fig. 1 nHAp and Ni^{+2} doped nHAp prepared using ammoniacal precipitation method.

4.2. EDAX

The extent of doping is a major concern for the metal doped bio ceramics, especially for metal ion doped hydroxyapatite. So far, many research groups have reported the synthesis of different metal ions (example cobalt, magnesium, zinc, iron) doped hydroxyapatite. A critical analysis of their results revealed that in most of the cases actual doping was less than the expected value (theoretical percentage doping). In the present study, the presence of dopant and extent of doping was confirmed by EDAX. The result showed that ammoniacal precipitation method can be successfully used for the doping of nickel in hydroxyapatite. It was observed that though there was a gradual increase in percentage doping with an increase of Ni^{+2} concentration in the precursor, however, the actual doping was less in comparison to the theoretical value (Fig.2). Analysis showed that in all cases the actual loading was less than 30% of the theoretical doping. In recent reports Guerra Lopez et.al, has shown that percentage doping for transition metals including nickel generally less than $1/3^{rd}$ of the theoretical doping. This happens probably because of the formation of stable amine co-ordination complex of Ni^{+2} at basic pH. That complex ions are generally much bigger in size, therefore, failed to get accommodated in the crystal lattice of hydroxyapatite[38]

4.3. TEM

The size of the hydroxyapatite nano crystal is very important for bone tissue application. In vivo, the nano hydroxyapatite is synthesized in situ during bone remodelling inside the grove of the collagen helices. The native size of hydroxyapatite nanocrystals lies between (2nm-10nm)[39].Here, TEM micrographs showed that the size of the synthesized doped HAp particles were all in nano range with an average diameter of15-17nm approximately(Fig.2).All the nanoparticles were found elliptical. The average ferret diameter for HAP was 17.2 ± 3.9 nm while the same for N1-HAP, N5-HAP and N10-HAP was 15.6 ± 3.3, 16.8± 3.0 and 15.1 ± 3.0 nm, respectively. Such a close value of the average ferret diameter of all the doped samples clearly implies that the doping of nickel has no significant impact on the size of the nano crystals.

Fig. 2. [A] FESEM micrographs of nHAp and Ni^{+2} doped nHAp. [B] TEM Images of nHAp and Ni^{+2} doped nHAp. [C] Nano particle size distribution. TEM Image based analysis was done using NIH-ImageJ software. For each analysis, 25 individual particles were considered ($p< 0.05$). [D] Percentage of Ni^{+2} doping with respect to calcium content (w/w). Results were expressed as Mean ± S.D of three independent experiments ($p <0.05$).

4.4. XRD

Analysis of the XRD profiles (Fig.3) of the doped HAp showed that there were no additional peaks corresponding to nickel. The characteristic peaks of HAp corresponding to 32°, 33° and 34° 2θ (for planes (211), (300) and (302) respectively) were found in all samples. Analysis of the crystal structure of the samples (Table.2) showed that the magnitude of the lattice parameter 'c' for HAP, N1-HAP and N5-HAP and N10-HAP were almost same. Further analysis showed that there was a decrease in crystallinity with an increase in doping percentage. In this present study, no such peak broadening was observed which implies that Ni^{+2} doping did not distort the apatite crystal much. However, the variation in crystal parameter observed was probably because of the smaller ionic radii of Ni^{+2} (0.72Å) in comparison to Ca^{+2} (0.99Å).

Table 2. Crystal parameters of nHAp and Ni^{+2} doped nHAp. Percentage crystallinity and d spacing were calculated using the XRD and TEM diffraction data corresponding to 002 planes. For the analysis of crystal lattice parameters, 'an' and 'c', 300 and 002 planes are considered.

S.No	Samples	% Crystallinity	Crystal lattice		'd'-spacing
1.	HA				4
2.	N1-H				2
3.	N5-H				4
4.	N10-HAP	22	9.43	6.90	0.3578

Data protected for publication

Please contact banerjeei@nitrkl.ac.in for details

4.5. FT-IR

The FTIR analysis of the samples revealed the characteristic peaks of hydroxyapatite (Fig.3) No major peak shift was observed in the nickel doped samples. The peaks at $630cm^{-1}$, $600cm^{-1}$ and $550cm^{-1}$ corresponding to free OH and υ_4 vibrational bands of a phosphate group

$(PO_4)^{3-}$ respectively appears less prominent as the doping increases and becomes merged with N10-HAP. Peaks for other bands like υ_3 stretching of $(PO_4)^{3-}$ (1100 - 1000 cm^{-1}) and $\upsilon_2$bending of $(PO_4)^{3-}$ (470cm^{-1}) also became less prominent as the doping increases. These results were found to be in accordance with Guerra-López et al. and G. Gergely et al.[38]. This maybe because of the mild variation in that ionic environment in the crystal lattice which leads to alteration in the stretching field. All the samples show a common peak of H-bonded OH stretching at 3570cm^{-1}. However in case of N5-HAP and N10-HAP, a new peak appeared at 3640cm^{-1} that could be attributed to the stretching of free OH, which becomes more intense with the increasing doping. Bands at 1470cm^{-1} and 870cm^{-1} corresponding to $(CO_3)^{2-}$ was seen due to the CO_2 adsorption from the atmosphere. Adsorbed water gave two kinds of the band, O-H bending (1640cm^{-1}) and O-H stretching (3450cm^{-1}) which was also due to the hydroxyl group present in the apatite. The peak at 1640cm^{-1} became wider in N10-HAP and N1-HAP, and this may be due to crystal deformation.

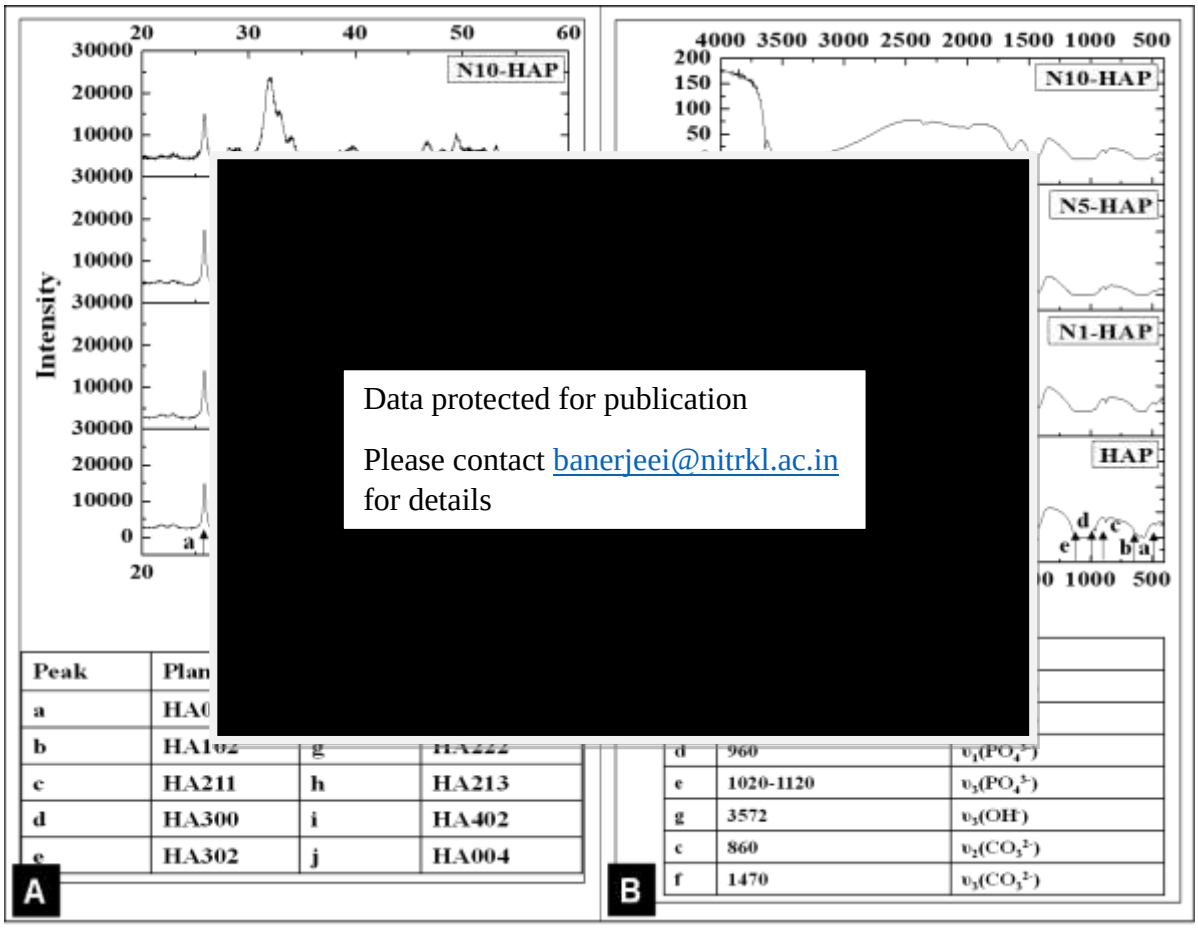

Fig. 3. [A] XRD analysis of nHAp and Ni^{+2} doped nHAp. Important characteristic peaks are marked in the figure, and its corresponding crystal planes were mention in the embedded table. [B] FT-IR analysis of nHAp and Ni^{+2} doped nHAp. Important characteristic peaks are marked in the figure, and its corresponding bond perturbation were mention in the embedded table.

4.6. BET Surface Area Analysis:

Large surface area is one of the key parameters why nanomaterials are highly reactive when compared micro or macro scale materials. For this reason, we analysed the surface area of the synthesized HAp samples. The surface area of pure HAP was found to be 109.120m^2/g and was in accordance with the previously reported value[40]. The same for N1-HAP, N5-HAP, and N10-HAP were 107.591m^2/g,111.732m^2/g and 83.165m^2/g respectively (Table 3). Our TEM study showed that the size of the nano particles for all samples were close. So it is

expected that the surface area of the nanomaterial should also be same unless there is a variation in the porosity of the synthesized materials. The BET study showed that there was no significance variation in surface area with doping which implies the doping has no significant effect on the porosity of the material.

4.7. Zeta potential of HAP particles:

The zeta potential of the nano materials influences the biological performance of the materials in a number of ways. It is already reported that in physiological condition, the zeta potential modulate protein adsorption, cell material interaction, and cellular uptake of the nano material. Doping of metal ions can change the normal zeta potential of hydroxyapatite by two ways: i) By altering the surface charge density ii) By imparting strain in the crystal that could lead to differential ion dissolution from a crystal. Here, the zeta potential of HAP was found to be -3.54mV and was found in accordance with former reports. It is also reported that the metal ion doping causes a variation in the zeta potentialin hydroxyapatite. However, the extent of such variation depends on the nature of the metal ion and extent of doping. Here, we have observed that with Ni^{+2} doping, the zeta becomes more positive in comparison to the HAP, and however there is no proportional increase in zeta with the increase in doping concentration (Table.3).

4.8. Protein adsorption:

The protein adsorption onto the implant plays a vital role in determining the host response towards the implant. There are number of plasma proteins (albumin, immunoglobins and fibrinogen, fibronectin) that interact with the biomaterial surface. Hence, BSA (Bovine

Serum Albumin) was used as a model protein to study the protein adsorption on the Ni doped hydroxyapatite. As reported earlier, protein adsorption by HAp depends on surface area and zeta potential more specifically on the charge distribution of the Ca/Ni and P ions over the crystal surface since Ca and P sites are the sites for the electrostatic adsorption of proteins [41]. Both HAp and doped Hap samples showed similar protein adsorption onto their surface (Table.3). The average protein adsorption was found in the range 900µg/10mg of the samples. The result clearly implied that the doping of nickel did not influence the protein adsorption capacity of hydroxyapatite nanoparticles.

Table 3. Analysis of surface area, pore volume, zeta potential and protein absorption. The data were mean of three independent experiments and presented as Mean ± S.D.

S.No	Samples	Surface area	Pore volume	Zeta potential	Protein adsorption g)
1.	H				19.5
2.	N1-				±7.4
3.	N5-				18.4
4.	N10-HAp	83.2	0.054	1.1	878.5±1.2

Data protected for publication

Please contact banerjeei@nitrkl.ac.in for details

4.9. MTT assay

During development, osteoblast cells are the one which first proliferates, then differentiates into osteocytes and produce an extracellular bone matrix. It is now well established that osteoblast proliferation is essential for the bone regeneration and remodelling. In this present study, the MTT assay was performed for the cells treated with Ni doped HAp samples (Fig.4). Pure HAp showed the highest cell proliferation in comparison to all other samples. The extent of cell growth was very much similar for all the samples on day 1. The

proliferation rate becomes slow from day 3 with N10-HAp giving the least cell growth. N1-HAP and N5-HAP showed similar proliferation rate as pure HAP on day 3 but on day 5 proliferation reduced when compared to pure HAP. This behaviour may be attributed to either nickel doping being cytotoxic to cells, or the cells are getting differentiated after day 3.

4.10. Cell cycle analysis

Cell cycle analysis (Fig.4) showed that nickel doping did not perturb normal cell cycle progression. For all the treatment groups, distribution of cell populations in different phases of cell cycle was similar to that of control (TCP) which indicates that nickel doping has no detrimental effect on viability and cell proliferation. For all the cases, highest cell population was observed in G_0/G1 phase (between 55-65%) except the cells treated with N5- HAP where percentage cell population in G0/G1 was even little higher. More interestingly, N5- HAP has least cell population in S phase (12%). On the other hand, least population in G_2/M phase was found in N10-HAP treated group. In bone physiology, a high population of cells in G_0/G_1 often indicates their commitment towards differentiation. Therefore, a higher value G_0/G_1 in case of N5-HAP treated group could be associated with differentiation potential of the material. FACS analysis also showed that the percentage cell population in pro G_0/G_1 (a phase associated with apoptosis) was negligible for all groups which imply that nickel doping has no adverse effect on the cell viability.

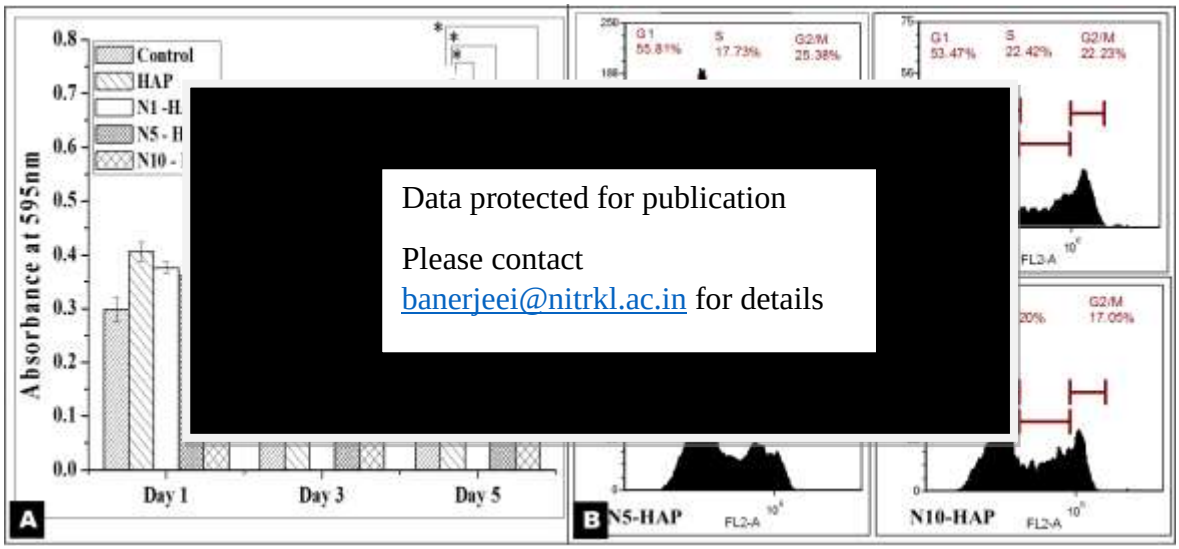

Fig. 4. [A] Study of cell proliferation by MTT assay. Data were expressed as Mean ± S.D (n=3). Statistical significance was checked for p< 0.005. [B] Study of the cell cycle after 24 h of treatment. Experiments were done in triplicate. Representative histograms for each sample was presented.

4.11. Live/Dead Assay:

It was evident from the literature that hydroxyapatite and doped hydroxyl apatite support osteoblast cell viability and proliferation in vitro for longer period. Our MTT analysis apparently showed Ni doped hydroxy apatite samples help in MG-63 cell proliferation. However, it is important to mention that, MTT assay is actually a measurement of the metabolic state of the cells and often fails to indicate cell proliferation effectively. Therefore, it was important to quantify the variation in a live population of cells. For this purpose, flow cytometry based Live / Dead assay was performed to determine the percentage of live cells in the total cell population after the treatment (Table.4). The result showed that the percentage of live cells in the total cell population for all the samples were more than 90%. This clearly suggests that Ni^{+2} doped hydroxyl apatite were as cytocompatible as control (synthetic hydroxyl apatite).Our MTT study showed that there was a decrease in cell proliferation rate with time. As mentioned earlier, the two possibilities could be either cell death or cell

differentiation. It was evident from the live dead assay that there was no significant cell death at the later phase of culture which clearly implied that the decrease in cell proliferation could be because of differentiation of cells in presence of doped nano hydroxy apatite.

Table 4. Analysis of the percentage of live cells after sample treatment. The assay was performed by flow cytometry using PI as a probe. Data were expressed as Mean± S.D (n=3).

Day	Live Dead Assay: Percentage of live cells				
	Control	**HAP**	**N1-HAP**	**N5-HAP**	**N10-HAP**
Day1					9±2.53
Day3					4±1.10
Day5					8±0.14

Data protected for publication

Please contact banerjeei@nitrkl.ac.in for details

4.12. Differentiation of osteoblasts

Osteoblast differentiation into osteocytes and its maturation were the main processes involved in the effective bone remodelling after bone matrix deposition and osteoblast proliferation. The inorganic components of bone (hydroxyapatite), extra cellular matrix and its components along with many different kinds of growth factors like bone morphogenic proteins (BMPs, epidermal growth factors (EGFs) , fibroblast growth factors(FGFs), and many more widely affect the osteoblast differentiation[41]. Transcription factor runx2 is one among the signature protein which is a pre-requisite for the mesenchymal stem cells to differentiate to osteoblast cells. It is important to mention that MG -63 is a mature osteoblast. Therefore, Runx2 expression always remains in basal level in MG-63 in comparison to its

progenitor. A qualitative analysis of immuno-cytochemistry micrograph showed that as per expectation Runx2 is not localized on cell nucleus (as the cells has passed their early differentiation phase) and distributed all over the cells. Quantitative Image analysis using NIH-Image J showed that variation in expression level of Runx2 in all samples were statistically insignificant. When checked at mRNA level by RT-PCR, it was observed that there was no sample specific variation in the expression of Runx2 (Fig.5). These two experiments altogether showed that the presence of nickel doesn't affect the expression of runx2.

SEM micrograph taken after 3 days of sample treatment showed clear evidence of bone matrix deposition and nodule formation in all samples (Fig.5). Previously, Gough et.al outlined that the formation of the nodule is a signature of osteoblast differentiation. N5-HAP showed bigger nodule formation when compared to all samples which implied its greater osteogenic property.

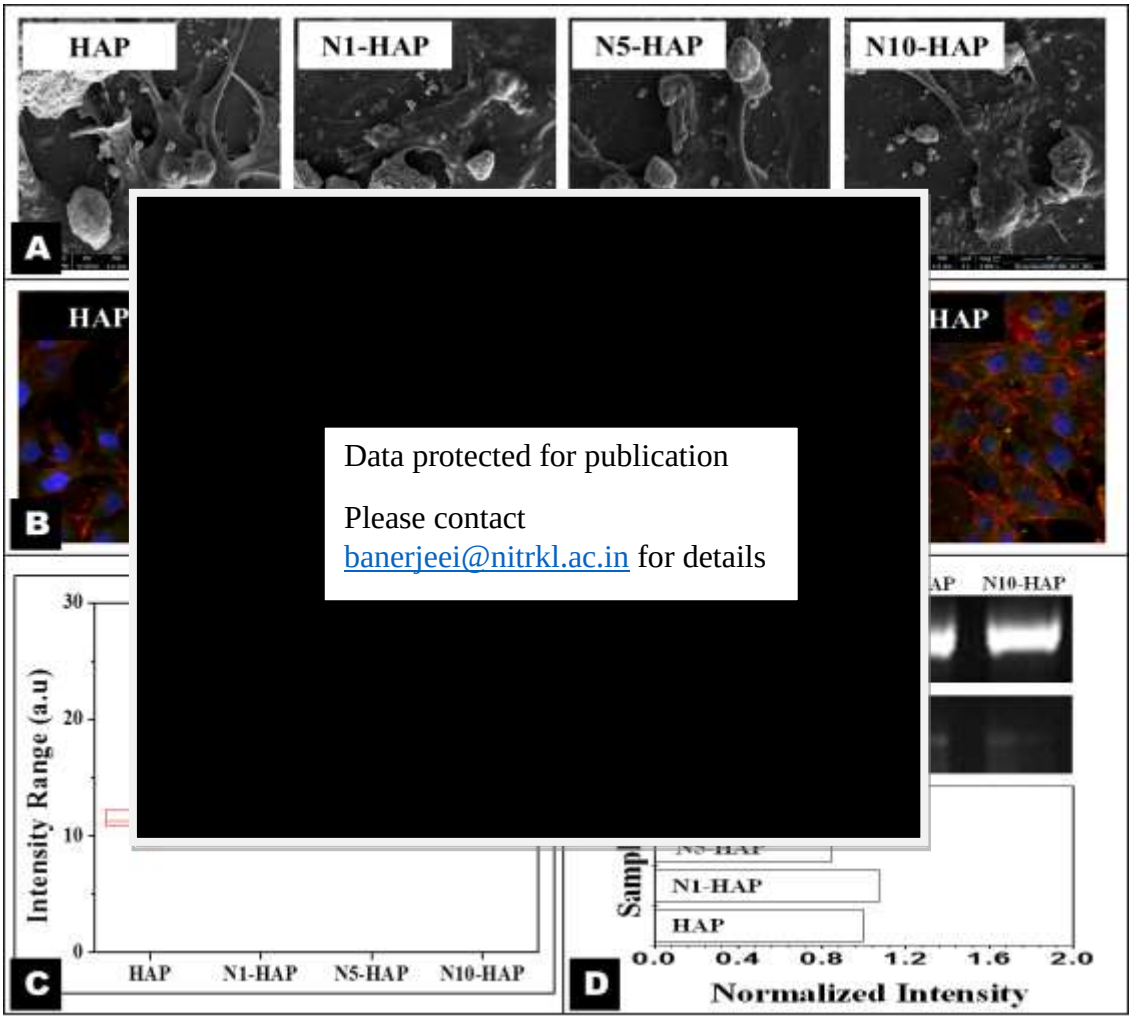

Fig. 5. [A] SEM images of cells cultured in presence of nHAp and Ni^{+2}doped nHAp samples at day 3. [B] Confocal micrographs of cells cultured in presence of nHAp and Ni^{+2}doped nHAp samples at day 3. Red [F actin], Blue [DAPI] and Green [Runx2]. [C] Quantitative image analysis of Runx 2 expression. Intensity was calculated for 10 cells. Statistical significance was checked for p< 0.005. [D] Study of Runx2 expression by RT-PCR.

4.13. Expression of VEGF

The expression of VEGF measured by ELISA (Fig.6) showed that there were a 2.3 fold, 3.5 fold and 3.8 fold increase in VEGF expression for N1-HAP, N5-Hap, N10-HAP treated group respectively, with respect to pure HAP after 48 h of treatment. Statistical analysis revealed that such increase in cellular VEGF expression with the increase in doping

concentration is statistically significant ($p<0.005$) for any two samples including control. RT-PCR based analysis of VEGF expression at mRNA level (Fig.6) further confirmed the increase in VEGF gene expression with the increase in Ni^{+2} doping concentration. An image based analysis of the intensity of the PCR bands (amplicons) showed that, in comparison to pure HAp, maximum expression was obtained for N10-HAP (fold) followed by N5-HAP (fold) and N1-HAP (fold) respectively.

4.14. Expression of HIF-1α

In this study, the immunocytochemistry profile of HIF-1α showed that the nickel doped HAp samples had a significantly higher expression of HIF-1α. In case of bone formation during embryogenesis, vascularisation of cartilage analague is a key step for further bone formation. Mesenchymal condensation Generally, under normoxic conditions, prolyl hydroxylase enzyme activates the proteosomal degradation pathway of HIF-1α through ubiquitination. Bivalent metal ions such as nickel, cobalt, copper, etc. mimics hypoxia condition by replacing Fe^{2+} ions, the key cofactor of the prolyl hydroxylase enzyme and thereby inactivating the enzyme and stabilizing HIF-1α. Interestingly, in this study, we observed that such expression level of HIF-1α did not show a linear trend with respect to nickel doping concentration (Fig.6). Generally, the release of ions and the degradation of HAp depends on its crystal structure (Ref.). Hence, the variation among the crystal structure of doped HAp might lead to variation in the nickel release and further HIF-1α expression. In case of HIF-1α expression, N5 showed the highest expression followed by N10, N1 and HAP, respectively. But in case of VEGF expression, the increase was linear with respect to nickel doping concentration. This might be explained on the basis that VEGF expression does not merely depend on the HIF-1α expression level. Apart from this, Lee et al. (2012) stated that Runx2 also stabilizes HIF-1α by competing with the Von Hippel-Lindau Protein (pVHL) (protein

that aids in proteosomal degradation of HIF-1α) and stabilizes HIF-1α protein. From the Runx2 immunocytochemistry expression profile, N5 showed better expression of Runx2 followed by N10. It was also reported for cu and co doped proangiogenic biomaterials VEGF expression profile not always follow the HIF-1α profile.

Fig. 6. [A] Study of VEGF expression by MG-63 cells. Cells were treated with Ni^{+2} doped nHAp for 48 h. Data are expressed as Mean ± S.D. [B] Study of VEGF mRNA expression by RT-PCR. [C] Study of HIF-1α expression by MG-63 cells after 12 h post treatment by immuno-cytochemistry. Confocal micrographs of the cells [Red (F actin), Blue (DAPI) and Green (HIF-1α)]. [D] Quantitative image analysis of HIF-1α expression. Intensity was calculated for 10 cells. Statistical significance was checked for p< 0.005. [E] Study of HIF-1α mRNA expression by RT-PCR.

CHAPTER 5

CONCLUSION

5. Conclusion:

Here we have reported the synthesis and characterization of Ni^{+2} doped nHAp and evaluation of its osteoconductive and proangiogenic properties. Bivalent nickel has been known as an inducer of cellular VEGF. We hypothesized that incorporation of Ni^{+2} into osteoconductive nHAp might convert it into a proangiogenic-osteogenic biomaterial. Our study showed that Ni^{+2} doped nHAp particles of the narrow size distribution could effectively be prepared by wet chemical precipitation method using CTAB. Doping of Ni^{+2} upto 3.3 % w/w of Ca^{+2} did not cause crystal deformation. Similarly, physical properties like surface area, zeta potential and protein absorption remained almost same with Ni^{+2} doping. All the doped samples were bone cell compatible and osteoconductive. Analysis showed that Ni^{+2} doped nHAp samples were a potent inducer of cellular VEGF, and the expression of VEGF was directly proportional to the doping concentration of Ni^{+2}. A mechanistic analysis further implied the involvement of Ni^{+2} in HIF-1α stabilization followed by increased VEGF expression. Comparison of these results with the relevant literature revealed number of important points. Firstly, although biological performance of the Ni^{+2} doped nHAp was similar to the other proangiogenic bio-ceramics (metal ion doped), i.e. all are osteoconductive as well as potent VEGF inducer, the relative VEGF expression per unit quantity of doping was higher in the present case. Secondly, the extent of nickel doping was less than all the reported values and below the toxic level. Finally, particle size was found within the range of 14-19 nm, which is good for bone tissue engineering. In conclusion, Ni^{+2} doped nHAp is a proangiogenic–osteogenic material and could be used in bone tissue engineering. The response of endothelial cells (viability and tube formation) against these materials *in vitro* has to be studied. Moreover, it is important to assess the biological performance of the materials *in vivo*.

CHAPTER 6

BIBLIOGRAPHY

6.BIBLIOGRAPHY

1. Buckwalter, J. and R. Cooper, *Bone structure and function.* Instructional course lectures, 1986. **36**: p. 27-48.
2. Hancox, N.M., *Biology of bone*. 1972: CUP Archive.
3. Towler, D.A., *Vascular biology and bone formation: hints from HIF*. Journal of Clinical Investigation, 2007. **117**(6): p. 1477.
4. Price, J., B. Oyajobi, and R. Russell, *The cell biology of bone growth.* European journal of clinical nutrition, 1994. **48**: p. S131-49.
5. Khan, S.N., et al., *The biology of bone grafting.* Journal of the American Academy of Orthopaedic Surgeons, 2005. **13**(1): p. 77-86.
6. Rose, F.R. and R.O. Oreffo, *Bone tissue engineering: hope vs hype.* Biochemical and biophysical research communications, 2002. **292**(1): p. 1-7.
7. Salgado, A.J., O.P. Coutinho, and R.L. Reis, *Bone tissue engineering: state of the art and future trends.* Macromolecular bioscience, 2004. **4**(8): p. 743-765.
8. Stevens, M.M., *Biomaterials for bone tissue engineering.* Materials today, 2008. **11**(5): p. 18-25.
9. Liu, X. and P.X. Ma, *Polymeric scaffolds for bone tissue engineering.* Annals of biomedical engineering, 2004. **32**(3): p. 477-486.
10. Burg, K.J., S. Porter, and J.F. Kellam, *Biomaterial developments for bone tissue engineering.* Biomaterials, 2000. **21**(23): p. 2347-2359.
11. Kay, M., R. Young, and A. Posner, *Crystal structure of hydroxyapatite.* 1964.
12. Suchanek, W. and M. Yoshimura, *Processing and properties of hydroxyapatite-based biomaterials for use as hard tissue replacement implants.* Journal of Materials Research, 1998. **13**(01): p. 94-117.
13. Ray, R.D., *Vascularization of bone grafts and implants.* Clinical orthopaedics and related research, 1972. **87**: p. 43-48.

14. Lee, K., E.A. Silva, and D.J. Mooney, *Growth factor delivery-based tissue engineering: general approaches and a review of recent developments.* Journal of the Royal Society Interface, 2011. **8**(55): p. 153-170.

15. Choong, C.S., D.W. Hutmacher, and J.T. Triffitt, *Co-culture of bone marrow fibroblasts and endothelial cells on modified polycaprolactone substrates for enhanced potentials in bone tissue engineering.* Tissue engineering, 2006. **12**(9): p. 2521-2531.

16. Santos, M.I. and R.L. Reis, *Vascularization in bone tissue engineering: physiology, current strategies, major hurdles and future challenges.* Macromolecular bioscience, 2010. **10**(1): p. 12-27.

17. Unger, R.E., et al., *Tissue-like self-assembly in cocultures of endothelial cells and osteoblasts and the formation of microcapillary-like structures on three-dimensional porous biomaterials.* Biomaterials, 2007. **28**(27): p. 3965-3976.

18. Schipani, E., et al., *Regulation of osteogenesis-angiogenesis coupling by HIFs and VEGF*. Journal of bone and mineral research, 2009. **24**(8): p. 1347-1353.

19. Wu, C., et al., *Hypoxia-mimicking mesoporous bioactive glass scaffolds with controllable cobalt ion release for bone tissue engineering.* Biomaterials, 2012. **33**(7): p. 2076-2085.

20. Wu, C., et al., *Copper-containing mesoporous bioactive glass scaffolds with multifunctional properties of angiogenesis capacity, osteostimulation and antibacterial activity*. Biomaterials, 2013. **34**(2): p. 422-433.

21. Monmaturapoj, N., *Nano-size hydroxyapatite powders preparation by wet-chemical precipitation route.* Journal of Metals, Materials and Minerals, 2008. **18**(1): p. 15-20.

22. Earl, J., D. Wood, and S. Milne. *Hydrothermal synthesis of hydroxyapatite*. in *Journal of Physics: Conference Series*. 2006. IOP Publishing.

23. Mobasherpour, I., et al., *Synthesis of nanocrystalline hydroxyapatite by using precipitation method.* Journal of Alloys and Compounds, 2007. **430**(1): p. 330-333.

24. Mayer, I., et al., *TEM study of the morphology of Mn 2+-doped calcium hydroxyapatite and β-tricalcium phosphate*. Journal of inorganic biochemistry, 2008. **102**(2): p. 311-317.

25. Li, Y., J. Ho, and C.P. Ooi, *Antibacterial efficacy and cytotoxicity studies of copper (II) and titanium (IV) substituted hydroxyapatite nanoparticles.* Materials Science and Engineering: C, 2010. **30**(8): p. 1137-1144.

26. Bose, S. and S.K. Saha, *Synthesis and characterization of hydroxyapatite nanopowders by emulsion technique.* Chemistry of materials, 2003. **15**(23): p. 4464-4469.

27. Lopes, M., et al., *Hydrophobicity, surface tension, and zeta potential measurements of glass-reinforced hydroxyapatite composites.* Journal of biomedical materials research, 1999. **45**(4): p. 370-375.

28. Luo, Q. and J.D. Andrade, *Cooperative adsorption of proteins onto hydroxyapatite.* Journal of colloid and interface science, 1998. **200**(1): p. 104-113.

29. Wang, H., et al., *Biocompatibility and osteogenesis of biomimetic nano-hydroxyapatite/polyamide composite scaffolds for bone tissue engineering.* Biomaterials, 2007. **28**(22): p. 3338-3348.

30. Adams, G.B., et al., *Stem cell engraftment at the endosteal niche is specified by the calcium-sensing receptor.* Nature, 2006. **439**(7076): p. 599-603.

31. Kim, H.-J., et al., *Selective neuronal degeneration induced by soluble oligomeric amyloid beta protein.* The FASEB Journal, 2003. **17**(1): p. 118-120.

32. Shi, Z., et al., *Size effect of hydroxyapatite nanoparticles on proliferation and apoptosis of osteoblast-like cells.* Acta biomaterialia, 2009. **5**(1): p. 338-345.

33. Chávez, J.C., et al., *Expression of hypoxia-inducible factor-1α in the brain of rats during chronic hypoxia.* Journal of Applied Physiology, 2000. **89**(5): p. 1937-1942.

34. Kumar-Singh, S., et al., *Angiogenic cytokines in mesothelioma: a study of VEGF, FGF-1 and-2, and TGF β expression.* The Journal of pathology, 1999. **189**(1): p. 72-78.

35. Shih, W.-J., M.-C. Wang, and M.-H. Hon, *Morphology and crystallinity of the nanosized hydroxyapatite synthesized by hydrolysis using cetyltrimethylammonium bromide (CTAB) as a surfactant.* Journal of Crystal Growth, 2005. **275**(1): p. e2339-e2344.

36. Stanić, V., et al., *Synthesis, characterization and antimicrobial activity of copper and zinc-doped hydroxyapatite nanopowders.* Applied Surface Science, 2010. **256**(20): p. 6083-6089.

37. Tank, K.P., et al., *Cobalt-doped nanohydroxyapatite: synthesis, characterization, antimicrobial and hemolytic studies.* Journal of nanoparticle research, 2013. **15**(5): p. 1-11.

38. Guerra-López, J., et al., *Influence of nickel on hydroxyapatite crystallization.* Journal of Raman Spectroscopy, 2001. **32**(4): p. 255-261.

39. Ahn, E.S., *Nanostructured apatites as orthopedic biomaterials*. 2001, Massachusetts Institute of Technology.

40. Puvvada, N., P.K. Panigrahi, and A. Pathak, *Room temperature synthesis of highly hemocompatible hydroxyapatite, study of their physical properties and spectroscopic correlation of particle size.* Nanoscale, 2010. **2**(12): p. 2631-2638.

41. Ducy, P., et al., *Osf2/Cbfa1: a transcriptional activator of osteoblast differentiation.* cell, 1997. **89**(5): p. 747-754.